Molecular-engineered hybrid carbon nanofillers for thermoplastic polyurethane nanocomposites with high mechanical strength and toughness

Le Li [a], Lin Xu [a], Wei Ding [a], Hengyi Lu [a], Chao Zhang [a,**], Tianxi Liu [a,b,c,*]

[a] State Key Laboratory for Modification of Chemical Fibers and Polymer Materials, College of Materials Science and Engineering, Innovation Center for Textile Science and Technology, Donghua University, Shanghai, 201620, PR China
[b] Key Laboratory of Synthetic and Biological Colloids, Ministry of Education, School of Chemical and Material Engineering, Jiangnan University, Wuxi, 214122, PR China
[c] Key Laboratory of Materials Processing and Mold (Zhengzhou University), Ministry of Education, Zhengzhou, 450002, PR China

ARTICLE INFO

ABSTRACT

The development of strong-yet-ductile polymer nanocomposites is critical, but still faces a great challenge. Herein, a hybrid carbon nanofiller consisting of one-dimensional carbon nanotube (CNT) and two-dimensional graphene (G) was molecularly engineered, and the as-prepared G-CNT hybrid nanofiller was then solution-casted with thermoplastic polyurethane (TPU) for the fabrication of TPU nanocomposite films. Due to the formation of unique network structure with multiple interactions of G-CNT hybrid within TPU matrices, the as-fabricated TPU nanocomposites showed simultaneously improved mechanical strength and toughness. With addition of only 1 wt% G-CNT hybrid, the tensile strength and toughness of TPU/(G-CNT) nanocomposite reached 69.5 MPa and 246.2 MJ m^{-3}, 1.9 and 2.9 times over that of neat TPU, respectively. The significant and simultaneous enhancement in mechanical strength and toughness of TPU nanocomposites is attributed to homogeneously distributed G-CNT hybrid and its unique energy dissipations due to factures at different deformation stages upon tensile deformation. The work therefore provides a simple and efficient strategy for fabricating mechanically strong and ductile polymer nanocomposites with molecular-engineered hybrid carbon nanofillers.

1. Introduction

Polymer nanocomposites have drawn much attention in recent years due to their integrated structural and functional performance in new-emerging applications of aerospace, electromagnetic shielding, anti-static material and energy conversion/storage [1–8]. Due to strong aggregation tendency of nanofillers within polymer matrices [9–13], it is critical to fabricate high-performance polymer nanocomposites by achieving a uniform dispersion of nanofillers in polymer matrices and strong interfacial interaction between nanofillers and polymer matrices, which are research hotspots in this field for recent years [14–18]. Interfacial engineering of interactions between nanofillers and polymer matrices provides a feasible way to construct high-performance polymer nanocomposites [19–23]. Specifically, when the interfacial interaction

between nanofillers and polymer matrices is strong, a high reinforcing effect of nanofillers can be achieved due to efficient load transferring upon tensile. However, in this case, high-modulus nanofillers will also greatly restrict the mobility of polymer chains, which will dramatically reduce the toughness of as-prepared polymer nanocomposites [17,24]. On the contrary, when the interfacial interaction between nanofillers and polymer matrices is weak, such weak interactions including π-π interfacial interaction [13], hydrogen bonding [12], metal-ligand coordination [19,25] and ionic bonding [5,15] make it impossible to form effective load transferring between nanofillers and polymer matrices, thus greatly weakening the reinforcement effect. However, fracture energy will be preferentially absorbed due to destroy of weak interfacial interactions between nanofillers and polymer matrices upon deformation, which is helpful to improve the toughness of as-prepared polymer

---

nanocomposites [26,27]. The most common methods to construct polymer nanocomposites with multiple interfacial structures have been developed by surface modifications of nanofillers with multi-level interfacial regions [28]. However, the surface functionalization of nanofillers relies too much on complex and energy-consuming organic synthesis methods, which greatly restricts low-cost and large-scale preparation and application of polymer nanocomposites. Therefore, the construction of polymer nanocomposites with multiple interfacial structures by a simple and controllable method shows very important research and application prospects, which has become a challenge in this field.

Carbon nanofillers, such as graphene (G) and carbon nanotube (CNT), are promising reinforcing nanofillers due to their large surface area, high modulus and strength [29–32]. The construction of G-CNT hybrid with G and CNT building blocks can effectively overcome easy aggregations of G and CNT themselves, thus maximizing their inherent excellent physical properties as reinforcing nanofillers. In recent years, various physical and chemical methods have been used to construct the G-CNT hybrid. Typically, an in-situ chemical vapor deposition (CVD) strategy was presented for in-situ growth of CNT on G substrates toward the preparation of G-CNT hybrid. However, the in-situ CVD growth of G-CNT hybrid requires high energy consumption, expensive instrument and complex preparation process, which is difficult to achieve large-scale and low-cost preparation of G-CNT hybrid materials. In addition, the graphitization degree of G-CNT hybrid nanofillers obtained by high-temperature CVD process is high, which makes it difficult to achieve uniform dispersion and form a strong interfacial interaction between nanofillers and polymer matrices among as-fabricated polymer nanocomposites [33,34]. Solution-processed assembly of the G and CNT provides a simple and efficient approach for construction of G-CNT hybrid with weak interfacial interactions such as π-π interfacial interaction and van der Waals force [35,36]. At present, the addition of G-CNT hybrid into polymer matrices facilitates largely enhanced mechanical strength and modulus of as-fabricated polymer nanocomposites. However, the improvement of toughness of polymer nanocomposites using the hybrid nanofillers is extremely unsatisfactory [36–38]. Therefore, it is of great significance and challenge to fabricate hybrid carbon nanofillers with tailored internal interactions, so as to achieve simultaneously strengthening and toughening effects on polymer matrixes.

Herein, we demonstrate a covalent-bonding strategy for the construction of unique hybrid carbon nanofiller consisting of 1D CNT and 2D G, thus forming a 3D network structure with multiple interactions. The as-obtained G-CNT hybrid shows uniform dispersion in polar solvents and polymer matrices. The unique hybrid carbon nanofiller network with multiple interactions of covalent bonding, π-π interaction and hydrogen bonding within thermoplastic polyurethane (TPU) matrices provides efficient energy dissipations under stress, enabling the as-obtained polymer nanocomposites with simultaneously and dramatically improved mechanical strength and toughness.

2. Materials and methods

2.1. Materials

Graphite oxide was prepared according to a modified Hummers' method [37]. Raw multi-walled carbon nanotubes (r-CNT, length: >10 μm, outer diameter: 20–30 nm) were purchased from Chengdu Organic Chemicals. Epichlorohydrin (CP) was purchased from Aladdin Chemicals. Polyester-type thermoplastic polyurethane (TPU, Estane 58277) was purchased from BF Goodrich Company. All the other reagents were supplied from Sinopharm Chemicals and used as received. Deionized (DI) water was used throughout the experiments.

2.2. Preparation of epoxy group-functionalized graphene oxide (epoxy-GO)

A uniform dispersion of graphene oxide (GO) in water at a concentration of $1.0 \, mg \, mL^{-1}$ was prepared by adding 100 mg of graphite oxide into 100 mL of water followed by ultrasonication for 30 min. Upon the pH value of the dispersion adjusted to 11 using 0.1 M NaOH solution, 10 mL of epichlorohydrin was added into the dispersion, and the mixed dispersion was heated at 60 °C for 8 h under stirring. Epoxy-GO was collected by filtration, washed with water and dried at 40 °C overnight in vacuum.

2.3. Preparation of carboxyl group-functionalized CNT (carboxyl-CNT)

The r-CNT (500 mg) was refluxed in 100 mL of concentrated nitric acid at 120 °C for 6 h. Upon cooling, the suspension was filtered and washed with water until pH value of filtrate was larger than 5. Carboxyl-CNT was collected by filtration, washed with water and dried at 80 °C overnight in vacuum.

The content of carboxylic acid groups on the carboxyl-CNT was quantitatively analyzed by the back titration method [39]. The carboxyl-CNT (100 mg) was added into 15 mL of 0.1 M NaOH solution and stirred for 48 h to allow carboxylic acid groups on the carboxyl-CNT to equilibrate with NaOH. The mixture was filtered, and then the filtrate was titrated with 0.1 M HCl to determine the excess amounts of NaOH in the solution as well as the content of carboxylic acid groups on the carboxyl-CNT.

2.4. Preparation of GO-CNT hybrid and G-CNT hybrid

The GO-CNT hybrid was prepared by adding 25 mg of epoxy-GO and 25 mg of carboxyl-CNT into 100 mL of water under sonication for 30 min. The pH value of the dispersion was adjusted to 11. After refluxed at 80 °C for 12 h, GO-CNT hybrid was collected by filtration with water and ethanol separately. G-CNT hybrid was prepared by chemical reduction of GO-CNT hybrid using hydrazine hydrates at 95 °C for 6 h. G-CNT hybrid was filtered and dried at 60 °C for 24 h in vacuum. Control sample of the G/CNT mixture was prepared by directly mixing chemically reduced epoxy-GO and carboxyl-CNT.

2.5. Fabrication of neat TPU, TPU/G, TPU/CNT, TPU/(G-CNT) and TPU/G/CNT nanocomposites

TPU pellets (0.5 g) was dissolved in 5 mL of DMF at 90 °C, while designed amounts of nanofillers were added into 10 mL of DMF under ultrasonication for 30 min. The mixed suspension was ultrasonicated for another 10 min and poured into an Al mold to evaporate the solvent at 80 °C. The TPU/G, TPU/CNT, TPU/(G-CNT) and TPU/G/CNT represent the nanocomposite films with an average thickness of ~200 μm, with addition of nanofillers of chemically reduced epoxy-GO (G), carboxyl-CNT, G-CNT hybrid and G/CNT mixture, respectively. Meanwhile, control sample of neat TPU was obtained under similar solution-casting method without addition of any nanofillers.

3. Results and discussion

The schematic of the preparation procedures of the G-CNT hybrid is illustrated in Fig. 1. First, epoxy-GO was obtained by the displacement reaction between epichlorohydrin and GO in alkaline (Fig. 1a). Second, carboxyl-CNT was prepared by the acid treatment of r-CNTs (Fig. 1b). Finally, epoxy-GO was mixed with carboxyl-CNT in alkaline, to achieve their covalent coupling into the GO-CNT hybrid. The GO-CNT hybrid was then chemically reduced into the G-CNT hybrid using hydrazine hydrates as reducing agents to remove the excessive oxygen-containing groups and improve the structural integrity of hybrid carbon nanofillers (Fig. 1c). Serious sediments of rGO and carboxyl-CNT in *N,N-*
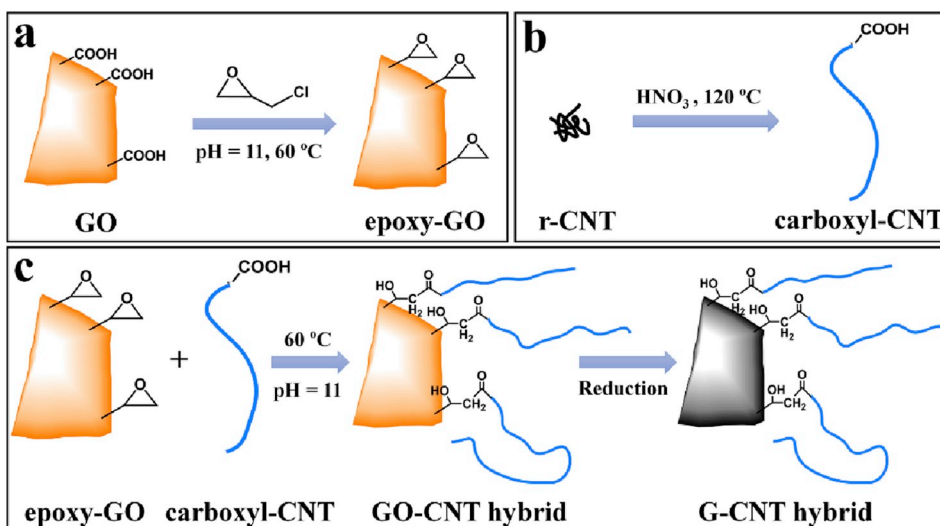
Fig. 1. Schematic of the preparation procedure of (a) epoxy-GO, (b) carboxyl-CNT and (c) G-CNT hybrid.

dimethylformamide (DMF) are observed at the bottom of vials after left-standing for 1 week (Fig. 2a). However, colloidal suspensions of as-prepared GO-CNT hybrid and G-CNT hybrid are well dispersed for 1 week in DMF (Fig. 2a), indicating that the G-CNT network structure largely inhibits the self-aggregation of rGO and carboxyl-CNT. The dispersions of the G-CNT hybrid in other representative organic solvents were investigated and summarized in Fig. S1. The dispersions of as-prepared G-CNT hybrid in acetone, n-methyl pyrrolidone (NMP) and tetrahydrofuran (THF) are observed to exhibit long-term stability comparable to that of the dispersion of G-CNT hybrid in DMF. Benefiting from the simple and efficient preparation procedure, the preparation of the G-CNT hybrid shows the potential to an up-scaled production. In one-batch preparation, the G-CNT hybrid can be dispersed in 1000 mL DMF at a concentration of $1 \, mg \, mL^{-1}$ (Fig. S2).

New-emerged characteristic peak ($\sim$1250 cm^{-1}) in the Fourier Transform infrared spectroscopy (FTIR) spectrum of epoxy-GO is

ascribing to C–O–C stretching vibration, indicating the successful grafting of epichlorohydrin onto GO (Fig. 2b). FTIR spectrum of pristine CNT shows weak absorption peaks centered at 1040 and 1582 cm^{-1}, corresponding to the existences of C–OH and C=C groups, respectively (Fig. S3). However, for the carboxyl-CNT, new absorption peaks at 1720 and 1228 cm^{-1} emerge (Fig. 2b), corresponding to the C=O and C–O–C stretching, respectively. The content of carboxyl acid groups on the surface of carboxyl-CNT is determined to be 6.2 $mmol \, g^{-1}$ by the back titration method. The surface of carboxyl-CNT can be successfully functionalized with abundant carboxyl acid groups through the nitric acid oxidation process. Moreover, FTIR spectrum of GO-CNT hybrid shows the appearance of C–OH stretching vibration ($\sim$1620 cm^{-1}) and the disappearance of C–O–C stretching vibration ($\sim$1250 cm^{-1}), indicating the formation of covalent bonding bridged with epichlorohydrin. The G-CNT hybrid shows largely decreased peak intensity at $\sim$3430 cm^{-1} ascribing –OH stretching vibration compared with that of
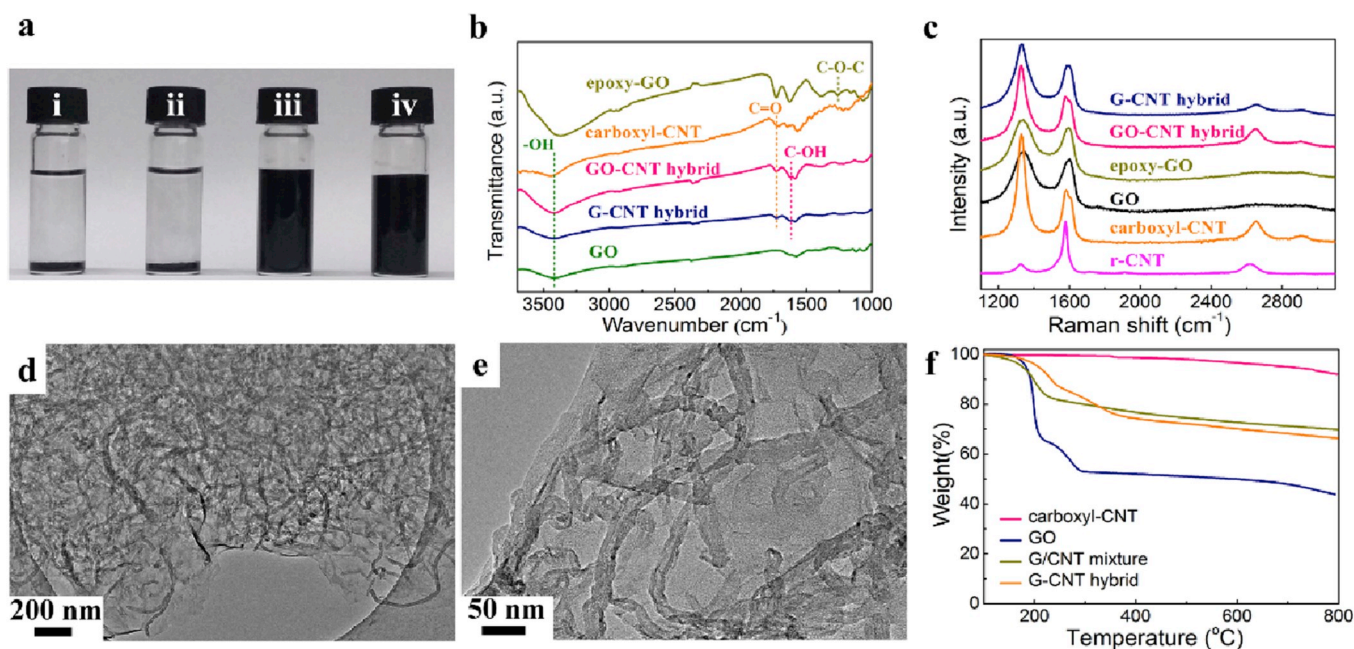

Fig. 2. (a) Photograph showing the dispersion of (i) carboxyl-CNT, (ii) G, (iii) GO-CNT hybrid and (iv) G-CNT hybrid at $1 \, mg \, mL^{-1}$ in DMF, left standing for 1 week. (b) FTIR spectra of epoxy-GO, carboxyl-CNT, GO-CNT hybrid, G-CNT hybrid and GO. (c) Raman spectra of G-CNT hybrid, GO-CNT hybrid, epoxy-GO, GO, carboxyl-CNT and r-CNT. TEM images of the G-CNT hybrid at (d) low and (e) high magnifications. (f) TGA curves of carboxyl-CNT, GO, G/CNT mixture and G-CNT hybrid.

GO-CNT hybrid, confirming the chemical reduction from GO-CNT hybrid to G-CNT hybrid. Raman spectra play an important role in detecting the structural evolutions of carbon materials. The GO shows the Raman spectrum with *D* and *G* bands at 1335 and 1604 cm^{-1}, respectively (Fig. 2c), corresponding to stretching of sp^3 and sp^2 carbon domains, respectively [40]. Compared with neat GO, Raman spectrum of epoxy-GO shows a similar I_D/I_G ratio, with *D* band slightly red-shifting to a low frequency. This is because the grafting occurring at GO edges through carboxyl acid groups would result in the change of graphitic carbon structure. The I_D/I_G ratio increases from 0.29 (r-CNT) to 2.08 (carboxyl-CNT), indicating the formation of abundant oxygen-containing groups on the carboxyl-CNT (Table S1). Interestingly, *D* and *G* bands of GO-CNT hybrid shift to 1335 and 1577 cm^{-1}, respectively, compared with that of epoxy-GO, clearly indicating the formation of large-sized in-plane sp^2 domains and the presence of π-π interaction between carboxyl-CNT and epoxy-GO [38].

Morphologies of G-CNT hybrid were investigated by transmission electron microscope (TEM) observations. Carboxyl-CNT is observed to be in their entangled forms (Fig. S4a), whereas the GO and epoxy-GO display stacked and wrinkled features (Figs. S4b and S4c). Interestingly, G-CNT hybrid clearly demonstrates homogeneous distributions of 1D CNTs on the surface of 2D G nanosheets, forming 3D interconnected network structure (Fig. 2d and e). The covalent bonding and π-π interaction between carboxyl-CNT and G inhibit their self-aggregations of CNT and G. The G-CNT hybrid shows an excellent structural stability without obvious changes during chemical reduction, compared with that of GO-CNT hybrid (Fig. S5). Thermal gravimetric analysis (TGA) measurements were conducted to investigate the thermal stability of G-CNT hybrid (Fig. 2f). A rapid mass loss between 200 and 300 °C is observed for the GO, attributing to the decomposition of oxygen-containing groups. The carboxyl-CNT exhibits a slight mass loss due to the decomposition of oxygen-containing groups within the defects among the CNT. The maximum degradation rate for G/CNT mixture occurs at 199 °C (Fig. S6). In contrast, a notable improvement in the thermal stability for G-CNT hybrid is observed, with maximum degradation rates for two main decomposition stages occurring at 227 °C and 311 °C, respectively (Fig. S6). The largely improved thermal stability for G-CNT hybrid is probably due to the presence of aromatic structures among G-CNT hybrid avoiding the decomposition of oxygen functional groups at the early low temperature [41]. All these results confirm the successful preparation of G-CNT hybrid with multiple interactions.

The G-CNT hybrid shows a uniform dispersibility in organic solvents, enabling its applications as a promising nanofiller for fabricating polymer nanocomposites. The TPU nanocomposites containing various nanofillers of carboxyl-CNT, G, G-CNT hybrid and G/CNT mixture were fabricated by the solution-casting method using the DMF as solvent. The dispersion of nanofillers within TPU nanocomposites is evaluated by TEM observations. TEM images of TPU/CNT and TPU/G nanocomposites show irregular aggregations of nanofillers (Fig. 3a–d). Conversely, the G-CNT hybrid shows a fine dispersion of both carboxyl-CNT and G (Fig. 3e). TEM image of TPU/(G-CNT) nanocomposite shows an interconnected G-CNT network structure with uniform dispersions of individual carboxyl-CNT surrounded by G throughout TPU matrices (Fig. 3f). The improved dispersion of G-CNT hybrid within TPU matrices, mainly attributing to strong interactions between carboxyl-CNT and G, is also reflected by largely enhanced mechanical properties of corresponding TPU nanocomposites.

Mechanical properties of neat TPU and its nanocomposites were evaluated using a universal material testing machine. Fig. 4a and b show typical stress-strain profiles, corresponding tensile strength and toughness of neat TPU and its nanocomposites. The tensile strength and toughness of neat TPU are only 36.2 MPa and 86.2 MJ m^{-3}, respectively. In contrast, the tensile strength and toughness of TPU/(G-CNT) (1 wt%) nanocomposite reach 69.5 MPa and 246.2 MJ m^{-3}, respectively, which are 1.9 and 2.9 times over that of neat TPU (Table 1). The significant improvement is also reflected on the tensile modulus of corresponding TPU nanocomposites, when compared to neat TPU. The above results are ascribed to the facts that the hybrid carbon nanofillers act as physical crosslinkers within TPU matrices. The increased crosslinking density may result in the formation of robust network structure among the TPU nanocomposites. Furthermore, the mechanical strength and toughness of TPU/(G-CNT) nanocomposites show remarkable improvements compared with that of TPU/G, TPU/CNT and TPU/G/CNT under the condition of the same nanofiller content, indicating unique and synergistic effects of G-CNT hybrid when reinforcing TPU matrices.

To quantify the synergistic effects on toughening of TPU nanocomposites, the synergy percentage (*S*) proposed by Prasadis is modified as follow [20]:

$$S = \frac{2KIC_{hy} - (KIC_G + KIC_{CNT})}{KIC_G + KIC_{CNT}}$$

where KIC_{hy}, KIC_G, and KIC_{CNT} represent the toughness of TPU/(G-CNT), TPU/G and TPU/CNT, respectively.

The TPU/G/CNT nanocomposite exhibits 13% improvement and 9% reduction in tensile strength and elongation at break, respectively, compared with that of neat TPU. The calculated toughness *S* for TPU/G/CNT is 29.5%. However, the tensile strength and elongation at break for TPU/(G-CNT) are simultaneously enhanced, and the toughness *S* for TPU/(G-CNT) is enhanced by 107.4% compared with that of TPU/G/CNT, confirming that extra covalent bonding among the G-CNT hybrid
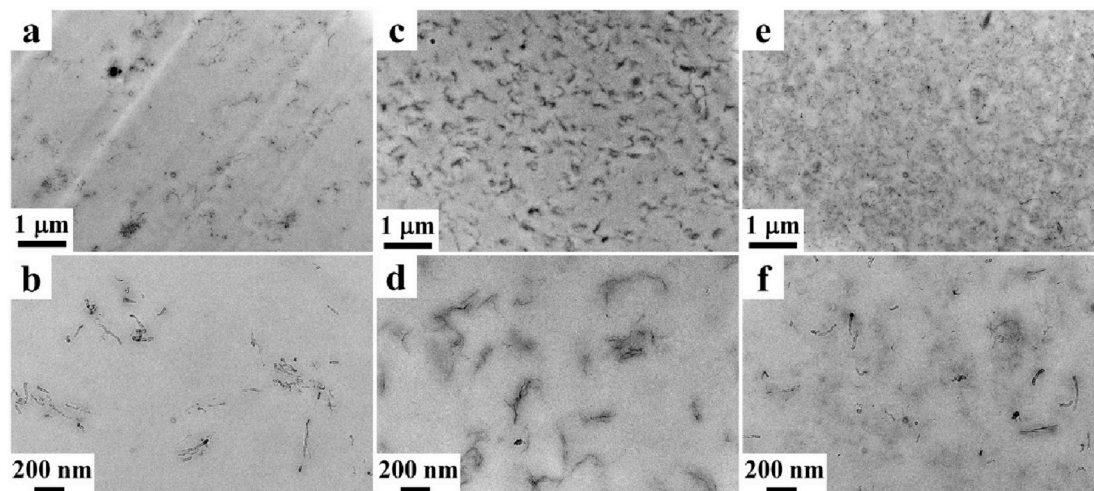

Fig. 3. TEM images of TPU nanocomposites containing 1 wt% (a, b) carboxyl-CNT, (c, d) G and (e, f) G-CNT hybrid, respectively.
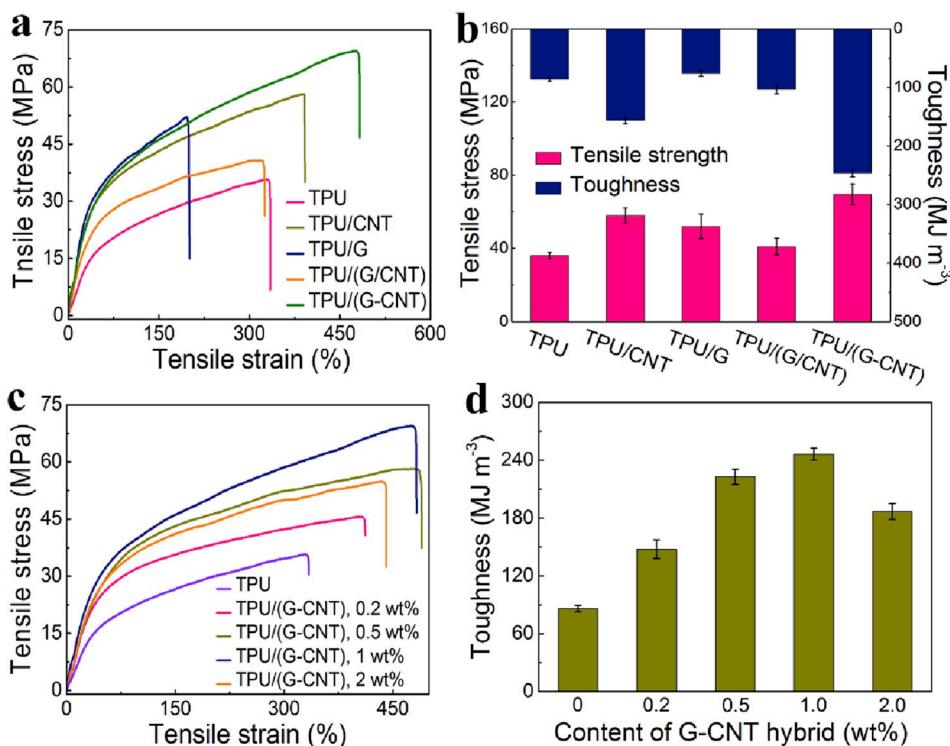
Fig. 4. (a) Typical tensile stress-strain curves, (b) tensile strength and toughness of neat TPU and its nanocomposites. (c) Typical tensile stress-strain curves, (d) toughness of neat TPU and TPU/(G-CNT) nanocomposites with various contents of G-CNT hybrid.

Table 1
Summary of mechanical properties of neat TPU and its nanocomposites.

Sample	Tensile strength (MPa)	Young's modulus (MPa)	Elongation at break (%)	Toughness (MJ m^{-3})
Neat TPU	36.2 ± 1.7	37.8 ± 4.7	351 ± 38	86.2 ± 3.3
TPU/CNT (1 wt%)	49.4 ± 4.1	68.4 ± 7.9	353 ± 25	131.7 ± 5.9
TPU/G (1 wt%)	52.1 ± 6.7	67.7 ± 9.1	195 ± 27	76.2 ± 5.0
TPU/G/CNT (1 wt%)	53.3 ± 4.5	68.3 ± 5.3	320 ± 46	134.7 ± 7.4
TPU/(G-CNT) (0.2 wt%)	45.7 ± 3.3	63.4 ± 8.5	496 ± 43	147.7 ± 9.6
TPU/(G-CNT) (0.5 wt%)	58.5 ± 3.2	75.3 ± 5.8	482 ± 35	222.8 ± 7.9
TPU/(G-CNT) (1 wt%)	69.5 ± 5.7	88.6 ± 8.7	475 ± 45	246.2 ± 6.3
TPU/(G-CNT) (2 wt%)	54.9 ± 4.2	68.5 ± 6.7	435 ± 22	186.8 ± 8.2

dramatically enhances synergistic toughening effects.

Mechanical properties of TPU/(G-CNT) nanocomposites with various nanofiller contents were further investigated. Fig. 4c and d show the influences of the G-CNT contents on mechanical strength and toughness of as-obtained TPU/(G-CNT) nanocomposites. The tensile strength and toughness of TPU/(G-CNT) nanocomposites considerably increase when the G-CNT content increases from 0.2 wt% to 1 wt%. However, the tensile strength and toughness of TPU/(G-CNT) nanocomposites obviously decrease when further increasing the G-CNT content to 2 wt% within TPU matrices. This is because the relatively high loading of G-CNT hybrid will cause their re-stacking within the TPU

and substantially weakened load transfer from TPU matrices to nanofillers.

Ex-situ FTIR spectra were conducted to monitor the interfacial interactions between the G-CNT hybrid and TPU matrices during tensile deformation (Fig. 5), to understand the fracture mechanism and toughness reinforcement of TPU/(G-CNT) nanocomposites. FTIR spectra of neat TPU and TPU/(G-CNT) nanocomposites were shown in Fig. 5a and b. FTIR spectrum of neat TPU exhibits sharp peaks at 3331, 1732 and 1597 cm^{-1}, corresponding to N–H groups, free and hydrogen bonded C=O groups in urethane linkage (–HN–COO-), respectively [42]. The variations in N–H (from 3331 to 3325 cm^{-1}) and C=O (from 1732 to 1728 cm^{-1}) peaks in the spectrum of TPU/(G-CNT) are attributed to the formation of hydrogen bonding interactions between the G-CNT hybrid and TPU matrices. Meanwhile, the intensity of absorption peak of free C=O groups (~1728 cm^{-1}) distinctly decreases, and the intensity of absorption peak of hydrogen bonded C=O groups (~1594 cm^{-1}) distinctly increases. These results indicate that abundant hydrogen bonding interactions exist between both the N–H and C=O groups of TPU matrices and oxygen functional groups of G-CNT hybrid. Ex-situ FTIR spectra were also conducted to monitor the molecular-level interactions of TPU/(G-CNT) nanocomposites under different tensile strains. As shown in Fig. 5c and d, the slight red shifting of the peaks ascribing to N–H and C=O groups indicates the breakage of hydrogen bonding upon stretching. Therefore, it can be concluded that the interfacial hydrogen bonding provides efficient energy dissipation pathway for remarkable toughness reinforcement.

Hysteresis behaviors of TPU/(G-CNT) nanocomposites during loading/unloading cycles were conducted to further understand the energy dissipations during tensile deformation. During stretching/recovery process, an obvious hysteresis loop is observed for TPU/(G-CNT) nanocomposites, and the areas of hysteresis loops (dissipated toughness) in loading/unloading curves reflect the energy dissipation ability. Comparison of stress-strain profiles and energy dissipations among TPU, TPU/CNT, TPU/G/CNT and TPU/(G-CNT) at the same strain (300%) were performed and displayed in Fig. 6a and b. The TPU/CNT, TPU/G/
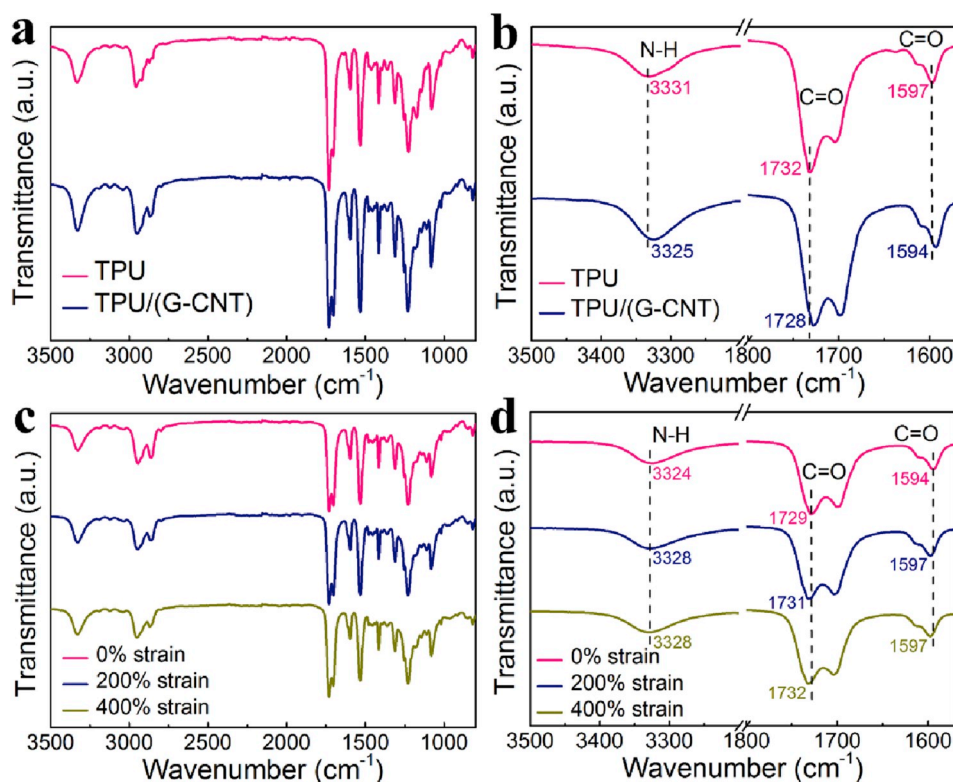
Fig. 5. (a) FTIR spectra of neat TPU and TPU/(G-CNT). (b) Enlarged FTIR spectra of TPU and TPU/(G-CNT) in the wavenumber range of 1800–1570 cm^{-1} and 3500–3200 cm^{-1}. (c) Ex-situ FTIR spectra of TPU/(G-CNT) under different tensile strains. (d) Enlarged ex-situ FTIR spectra of TPU/(G-CNT) in the wavenumber range of 1800–1570 cm^{-1} and 3500–3200 cm^{-1}.

CNT and TPU/(G-CNT) show relatively large hysteresis loops, while neat TPU displays unremarkable hysteresis loop. Consistently, the dissipated toughness of TPU/CNT (60.9 MJ m^{-3}), TPU/G/CNT (77.3 MJ m^{-3}) and TPU/G-CNT (98.6 MJ m^{-3}) are much higher than that of neat TPU (33.0 MJ m^{-3}) (Fig. 6b). This result indicates that the TPU/(G-CNT) nanocomposites possess most effective energy dissipations during tensile deformation, where covalent bonding and hydrogen bonding interactions played pivotal roles. Fig. 6c displays loading/unloading profiles of TPU/(G-CNT) nanocomposites at various strains. Generally, the dissipated toughness increases with increased strain. The TPU/(G-CNT) nanocomposites exhibit a dissipated toughness of 3.3 MJ m^{-3} at a strain of 50%, which is only 35.2% of the total toughness (Fig. 6d). In contrast, when the strain increases to 400%, the dissipated toughness of TPU/(G-CNT) reaches to 146.2 MJ m^{-3} (Fig. 6d), which is 77.9% of the total toughness. These results clearly indicate the formation of multiple interaction networks among the TPU/G-CNT nanocomposites. When the external loading is applied on the TPU/(G-CNT) nanocomposites, hydrogen bonding interaction first cracks to effectively dissipate energy, followed by fracture of covalent bonding interaction. Hence, the introduction of extra covalent bonding interaction among the G-CNT hybrid dramatically improves energy dissipations, thus enhancing the toughness of nanocomposites.

The proposed fracture mechanism accounting for remarkably toughening effects of G-CNT hybrid for TPU/(G-CNT) nanocomposites is proposed in Fig. 6e. Unique network structure with multiple interactions of both the covalent bonding and π-π interaction exists among the G-CNT hybrid, while coiled TPU chains penetrate into 3D G-CNT hybrid network due to hydrogen bonding. The G-CNT hybrid with multiple interactions endows as-fabricated TPU nanocomposites with hierarchical interfacial structures under stress. When the loading is applied (Stage I), most of energy is first transferred by forcing alignments of TPU chains along the loading direction, followed by further dissipation of large amounts of energy due to destruction of hydrogen bonding between TPU

chains and G-CNT hybrid. When the loading further increases (Stage II), more energy is dissipated due to fracture of unique hybrid network with multiple interactions in sequences of π-π interaction and covalent bonding between the carboxyl-CNT and G. The hierarchical interfaces with the synergistic interactions (hydrogen bonding, π-π interaction and covalent bonding) endow the TPU/(G-CNT) nanocomposites with substantial improvements in both mechanical strength and toughness.

Considering that the unique interfacial interactions among the TPU/ (G-CNT) nanocomposites including multiple non-covalent interactions, we further carried out the loading/unloading tests at a strain of 400% to evaluate the self-recoverability of TPU/(G-CNT) nanocomposites without external stimuli (Fig. 7a and b). In details, successive loading/ unloading tests with different rest time were conducted on TPU/(G-CNT) nanocomposites. The TPU/(G-CNT) nanocomposites show excellent self-recovery properties, and the recovery rates of tensile strength and dissipated energy of TPU/(G-CNT) increase with the increased rest time. When the second test was conducted immediately, the tensile strength recovered to 63% of its original value, and the dissipated energy recovered to 53% of its original value. When the second test was conducted after 4 h, the recovery ratios of tensile strength and dissipated energy were 87% and 82%, respectively. The internal network damage was better recovered with prolonging the rest time before reloading. This result ascribes to the reversible hydrogen-bonding interaction between the TPU and G-CNT hybrid. The excellent self-recoverability of TPU/(G-CNT) also indicates the favorable fatigue resistance of TPU/(G-CNT) nanocomposites at the same conditions.

Thermal stabilities of neat TPU and its nanocomposites with various nanofillers are shown in Fig. S7 and summarized in Table S2. The onset decomposition temperature ($T_{d(10\%)}$, temperature with a 10 wt% weight loss) of neat TPU is 330.4 °C due to the depolymerization of urethane bonding of TPU [43,44]. The maximum degradation rates for two main decomposition stages occur at 386 °C and 425 °C respectively (Fig. S7b), corresponding to the thermal degradation of soft segments within TPU
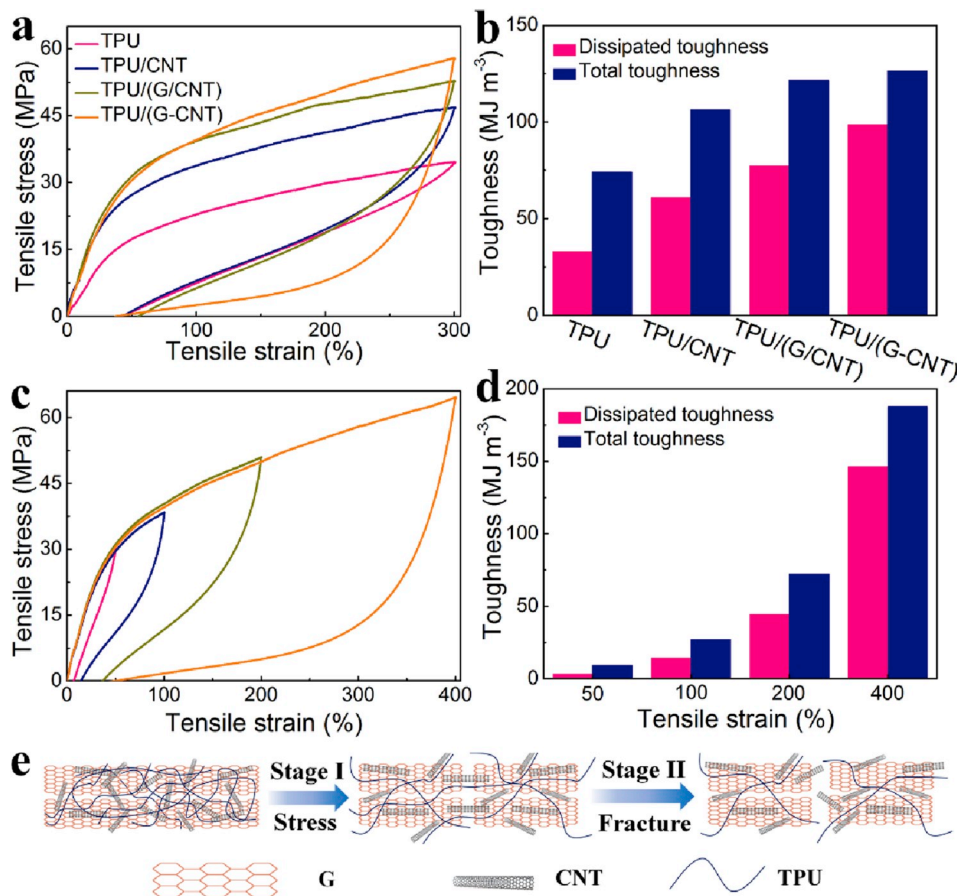
Fig. 6. (a) Loading/unloading tests of TPU, TPU/CNT, TPU/G/CNT and TPU/(G-CNT) under 300% strain. (b) The dissipated and total toughness calculated from (a). (c) Loading/unloading tests of TPU/(G-CNT) nanocomposites under different strains. (d) The dissipated and total toughness of calculated from (c). (e) The proposed fracture mechanism of TPU/(G-CNT) nanocomposites under tensile deformation.
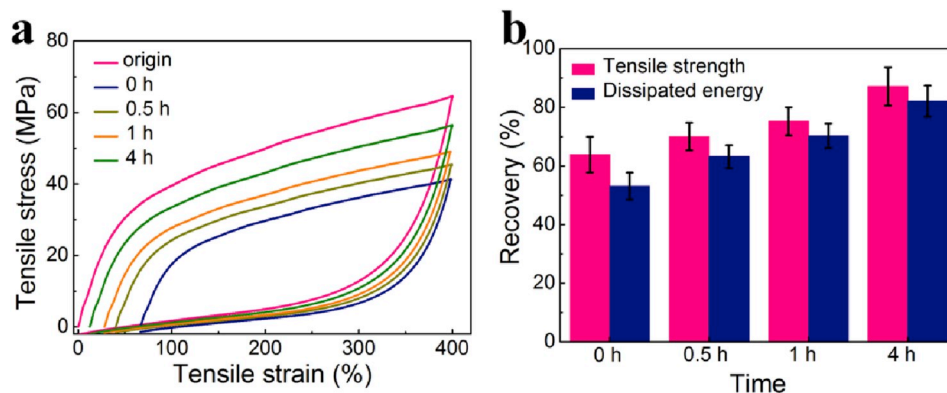

Fig. 7. Self-recovery tests of TPU/(G-CNT). (a) Successive loading/unloading tests of TPU/(G-CNT) with different rest time. (b) Time dependent recovery of tensile strength and dissipated energy of TPU/(G-CNT).

[44]. Further degradation at higher temperatures involves the decompositions of urea and isocyanate derivatives [43,44]. The decomposition temperature ($T_{d(50\%)}$, temperature with a 50 wt% weight loss) of TPU/(G-CNT) nanocomposites exhibits an increase of 18.4 °C compared with that of neat TPU, due to excellent thermal stability of G-CNT hybrid and its strong hindrances on TPU chain movements. Further, an improvement in the $T_{d(50\%)}$ of TPU/(G-CNT) nanocomposites is observed compared to that of TPU/CNT, TPU/G and TPU/G/CNT nanocomposites.

4. Conclusions

Unique hybrid carbon nanofillers consisting of 1D CNT and 2D G with multiple interfacial interactions including π-π interaction and covalent bonding were rationally designed and prepared. Due to multiple interfacial interactions within the G-CNT hybrid as well as their uniform dispersion and strong interfacial interaction within TPU matrices, the as-obtained TPU/(G-CNT) nanocomposite with 1 wt% nanofiller loading presented outstanding mechanical performance with much improved tensile strength (69.5 MPa) and toughness (246.2 MJ m^{-3}), increased by

92% and 186% compared with that of neat TPU. The controllable preparation of G-CNT hybrid with multiple interactions thus provides a simple and efficient approach for developing strong and ductile polymer nanocomposites for various structural and functional applications.

Acknowledgements

Appendix A. Supplementary data

Supplementary data to this article can be found online at https://doi.org/10.1016/j.compositesb.2019.107381.

References

[1] Zhao W, Kong J, Liu H, Zhuang Q, Gu J, Guo Z. Ultra-high thermally conductive and rapid heat responsive poly(benzobisoxazole) nanocomposites with self-aligned graphene. Nanoscale 2016;8(48):19984–93.

[2] Xiao H, Xie P, Qiu SJ, Rong MZ, Zhang MQ. Ultrathin-graphite foam with high mechanical resilience and electroconductibility fabricated through morphology-controlled solid-state pyrolysis of polyaniline foam. Carbon 2018;139:648–55.

[3] Liang X, Cheng Q. Synergistic reinforcing effect from graphene and carbon nanotubes. Compos Commun 2018;10:122–8.

[4] Li L, Wang K, Huang ZQ, Zhang C, Liu TX. Highly ordered graphene architectures by duplicating melamine sponges as a three-dimensional deformation-tolerant electrode. Nano Res 2016;9(10):2938–49.

[5] Gong S, Cheng Q. Bioinspired graphene-based nanocomposites via ionic interfacial interactions. Compos Commun 2018;7:16–22.

[6] Zhang QQ, Li Y, Feng YY, Feng W. Electropolymerization of graphene oxide/polyaniline composite for high-performance supercapacitor. Electrochim Acta 2013;90:95–100.

[7] Cha J, Jun GH, Park JK, Kim JC, Ryu HJ, Hong SH. Improvement of modulus, strength and fracture toughness of CNT/epoxy nanocomposites through the functionalization of carbon nanotubes. Compos Part B 2017;129:169–79.

[8] Hassanzadeh-Aghdam MK, Mahmoodi MJ, Ansari R. Creep performance of CNT polymer nanocomposites-An emphasis on viscoelastic interphase and CNT agglomeration. Compos Part B 2019;168:274–81.

[9] Rafiee MA, Rafiee J, Wang Z, Song H, Yu ZZ, Koratkar N. Enhanced mechanical properties of nanocomposites at low graphene content. ACS Nano 2009;3(12):3884–90.

[10] Feng YY, Zhang XQ, Shen YT, Yoshino K, Feng W. A mechanically strong, flexible and conductive film based on bacterial cellulose/graphene nanocomposite. Carbohydr Polym 2012;87(1):644–9.

[11] Wang M, Duan X, Xu Y, Duan X. Functional three-dimensional graphene/polymer vomposites. ACS Nano 2016;10(8):7231–47.

[12] Huang J, Zhang L, Tang Z, Guo B. Bioinspired engineering of sacrificial bonds into rubber networks towards high-performance and functional elastomers. Compos Commun 2018;8:65–73.

[13] Chen ZX, Lu HB. Constructing sacrificial bonds and hidden lengths for ductile graphene/polyurethane elastomers with improved strength and toughness. J Mater Chem 2012;22(25):12479–90.

[14] Wang Z, Tang XZ, Yu ZZ, Guo P, Song HH, Du XS. Dispersion of graphene oxide and its flame retardancy effect on epoxy nanocomposites. Chin J Polym Sci 2011;29(3):368–76.

[15] Jia LC, Sun WJ, Zhou CG, Yan DX, Zhang QC, Li ZM. Integrated strength and toughness in graphene/calcium alginate films for highly efficient electromagnetic interference shielding. J Mater Chem C 2018;6(34):9166–74.

[16] Chen Y, Zhang HB, Wang M, Qian X, Dasari A, Yu ZZ. Phenolic resin-enhanced three-dimensional graphene aerogels and their epoxy nanocomposites with high mechanical and electromagnetic interference shielding performances. Compos Sci Technol 2017;152:254–62.

[17] Guo BC, Tang ZH, Zhang LQ. Transport performance in novel elastomer nanocomposites: mechanism, design and control. Prog Polym Sci 2016;61:29–66.

[18] Cha J, Kim J, Ryu S, Hong SH. Comparison to mechanical properties of epoxy nanocomposites reinforced by functionalized carbon nanotubes and graphene nanoplatelets. Compos Part B 2019;162:283–8.

[19] Zhang X, Liu J, Zhang Z, Wu S, Tang Z, Guo B, et al. Toughening elastomers using a mussel-inspired multiphase design. ACS Appl Mater Interfaces 2018;10(28):23485–9.

[20] Gong S, Cui W, Zhang Q, Cao A, Jiang L, Cheng Q. Integrated ternary bioinspired nanocomposites via synergistic toughening of reduced graphene oxide and double-walled carbon nanotubes. ACS Nano 2015;9(12):11568–73.

[21] Gu J, Li Y, Liang C, Tang Y, Tang L, Zhang Y, et al. Synchronously improved dielectric and mechanical properties of wave-transparent laminated composites combined with outstanding thermal stability by incorporating iysozyme/POSS functionalized PBO fibers. J Mater Chem C 2018;6(28):7652–60.

[22] Gu H, Ma C, Liang C, Meng X, Gu J, Guo Z. A low loading of grafted thermoplastic polystyrene strengthens and toughens transparent epoxy composites. J Mater Chem C 2017;5(17):4275–85.

[23] Minář J, Brožek J, Michalcová A, Hadravová R, Slepička P. Functionalization of graphene oxide with poly(Í-caprolactone) for enhanced interfacial adhesion in polyamide 6 nanocomposites. Compos Part B 2019;174:107019.

[24] Zakaria MR, Abdul Kudus MH, Md Akil H, Mohd Thirmizir MZ. Comparative study of graphene nanoparticle and multiwall carbon nanotube filled epoxy nanocomposites based on mechanical, thermal and dielectric properties. Compos Part B 2017;119:57–66.

[25] Tang Z, Huang J, Guo B, Zhang L, Liu F. Bioinspired engineering of sacrificial metal–ligand bonds into elastomers with supramechanical performance and adaptive recovery. Macromolecules 2016;49(5):1781–9.

[26] Huang YF, Zhang MQ, Ruan WH. High-water-content graphene oxide/polyvinyl alcohol hydrogel with excellent mechanical properties. J Mater Chem A 2014;2(27):10508–15.

[27] Wen Y, Yin Q, Jia H, Yin B, Zhang X, Liu P, et al. Tailoring rubber-filler interfacial interaction and multifunctional rubber nanocomposites by usage of graphene oxide with different oxidation degrees. Compos Part B 2017;124:250–9.

[28] Zare Y, Rhee KY, Hui D. Influences of nanoparticles aggregation/agglomeration on the interfacial/interphase and tensile properties of nanocomposites. Compos Part B 2017;122:41–6.

[29] Yang WX, Zhang Y, Liu TY, Huang R, Chai SG, Chen F, et al. Completely green approach for the preparation of strong and highly conductive graphene composite film by using nanocellulose as dispersing agent and mechanical compression. ACS Sustainable Chem Eng 2017;5(10):9102–13.

[30] Feng W, Long P, Feng Y, Li Y. Two-dimensional fluorinated graphene: synthesis, structures, properties and applications. Adv Sci 2016;3(7):1500413.

[31] Yang M, Zhao N, Cui Y, Gao W, Zhao Q, Gao C, et al. Biomimetic architectured graphene aerogel with exceptional strength and resilience. ACS Nano 2017;11(7):6817–24.

[32] Ji TX, Feng YY, Qin MM, Feng W. Thermal conducting properties of aligned carbon nanotubes and their polymer composites. Compos Part A 2016;91:351–69.

[33] Shi J, Li X, Cheng H, Liu Z, Zhao L, Yang T, et al. Graphene reinforced carbon nanotube networks for wearable strain sensors. Adv Funct Mater 2016;26(13):2078–84.

[34] Ding Y-L, Kopold P, Hahn K, van Aken PA, Maier J, Yu Y. Facile solid-state growth of 3D well-interconnected nitrogen-rich carbon nanotube–graphene hybrid architectures for lithium–sulfur batteries. Adv Funct Mater 2016;26(7):1112–9.

[35] Zhang C, Ren LL, Wang XY, Liu TX. Graphene oxide-assisted dispersion of pristine multiwalled carbon nanotubes in aqueous media. J Phys Chem C 2010;114(26):11435–40.

[36] Liu MK, Zhang C, Tjiu WW, Yang Z, Wang WZ, Liu TX. One-step hybridization of graphene nanoribbons with carbon nanotubes and its strong-yet-ductile thermoplastic polyurethane composites. Polymer 2013;54(12):3124–30.

[37] Zhang C, Huang S, Tjiu WW, Fan W, Liu TX. Facile preparation of water-dispersible graphene sheets stabilized by acid-treated multi-walled carbon nanotubes and their poly(vinyl alcohol) composites. J Mater Chem 2012;22(6):2427–34.

[38] Roy S, Srivastava SK, Pionteck J, Mittal V. Mechanically and thermally enhanced multiwalled carbon nanotube–graphene hybrid filled thermoplastic polyurethane nanocomposites. Macromol Mater Eng 2015;300(3):346–57.

[39] Kar P, Choudhury A. Carboxylic acid functionalized multi-walled carbon nanotube doped polyaniline for chloroform sensors. Sens Actuators B Chem 2013;183:25–33.

[40] Zhou Y, Li L, Chen Y, Zou HW, Liang M. Enhanced mechanical properties of epoxy nanocomposites based on graphite oxide with amine-rich surface. RSC Adv 2015;5(119):98472–81.

[41] Dong B, Gwee L, Salasde lCD, Winey KI, Elabd YA. Super proton conductive high-purity nafion nanofibers. Nano Lett 2010;10(9):3785.

[42] Bian J, Lin HL, He FX, Wei XW, Chang IT, Sancaktar E. Fabrication of microwave exfoliated graphite oxide reinforced thermoplastic polyurethane nanocomposites: effects of filler on morphology, mechanical, thermal and conductive properties. Compos Part A 2013;47:72–82.

[43] Kotal M, Kuila T, Srivastava SK, Bhowmick AK. Synthesis and characterization of polyurethane/Mg-Al layered double hydroxide nanocomposites. J Appl Polym Sci 2009;114(5):2691–9.

[44] Chattopadhyay DK, Webster DC. Thermal stability and flame retardancy of polyurethanes. Prog Polym Sci 2009;34(10):1068–133.